

AT/VLTI field of view effect on MIDI data quality

C. Hummel, T. Rivinius, A. Kaufer, S. Morel (PSO)
I. Percheron (DFO), M. Wittkowski (USD)

March 27, 2006

1 Summary

The purpose of this report is an assessment of the quality of the MIDI/AT service mode data taken in P76 without the use of the variable curvature mirror (VCM).

All MIDI data (PRISM/HIGH.SENS) taken without operational VCMs were processed with regular (MIA+EWS Version 1.3, Jaffe et al. 2006, <http://www.strw.leidenuniv.nl/~nevec/MIDI/index.html>) and modified software routines (OYSTER/MYMIDIGUI, based on MIA+EWS, Hummel 2006, <http://www.sc.eso.org/~chummel/midi/mymidigui/mymidigui.html>) (Other modes such as GRISM and SCI_PHOT were not considered for this report because there were few observations using these.)

Even with the improved software routines many data sets are obviously faulty (visibility larger than unity) and/or noisy. Further improvements might be possible by a better fine-tuning of the parameters of the newly introduced algorithms. Despite these limitations some of these data would still have scientific value.

In P76, 88 MIDI/AT science OBs out of a total of 231 (32 of 50 in A-queue) were successfully executed with the use of the VCMs (on delay lines 5 and 6). The quality of some of these data (with the use of the VCM) was inspected, and appears to be of acceptable quality.

2 Operational limitations

It was very tricky, if not impossible, to operate MIDI at the ATs without the VCMs, in a manner to produce reliable results. In the case of the “zero” FOV, the MIDI acquisition had to be done using adjustments of M10, normally used to align the pupil. Offsets to the guiding position normally used to do the MIDI acquisition were now used to maximize the flux transmitted through the FOV. Errors in the M10 alignment cause mismatches of the beam overlap, decreasing fringe contrast.

In the case of the near-zero FOV, an additional complication arises from the photometric distortions which interfere with the acquisition since peak position is not computed reliably (which it can for the other case).

The variation in the quality of the acquisition is reflected in the inhomogeneity of the results. It is to be noted that the acquisition always used the IRIS detector, but even then the the maximum of flux found on IRIS did not always correspond to the maximum of flux on MIDI. For as yet unexplained reasons, the conditions that allow acquisition even without the VCMs as established during commissioning were not reproducible over the period.

3 Acquisition

It is important to realize that the sky emission is orders of magnitudes above the target signal, and the tunnel emission even surpasses the sky. However, the emission towards empty sky is also increased by the reflection losses at the many mirrors in between MIDI and the sky (see Fig. 1).

MIDI acquisition with the small field of view (FOV) delivered by the ATs without VCM is difficult since the target is either visible “behind” the (stationary) FOV or not, in which case it has to be searched for. To illustrate the (ideal) situation with a UT and a VCM-equipped AT, Fig. 2 shows representative (chopped) frames.

The acquisition during the AT/MIDI runs so far is characterized by a small or nearly zero FOV. In the first case, strong artefacts can be seen close to the (putative) target signal itself (e.g. negative “holes”, see Fig. 3), in the second case light can be either seen or not, but has always the same peaked profile. The artifacts can make the acquisition impossible since they dominate the target.

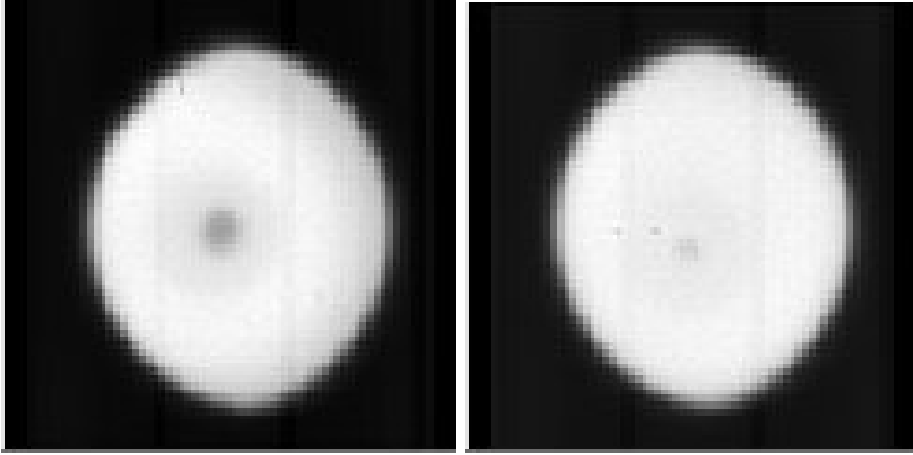


Figure 1: AT1 (left) and AT3 (right) FOV, as seen in the raw acquisition frames. The AT1 has noticeably more FOV as evidenced by the significant dip (about 20%) in the emission, while the AT3 field is nearly zero.

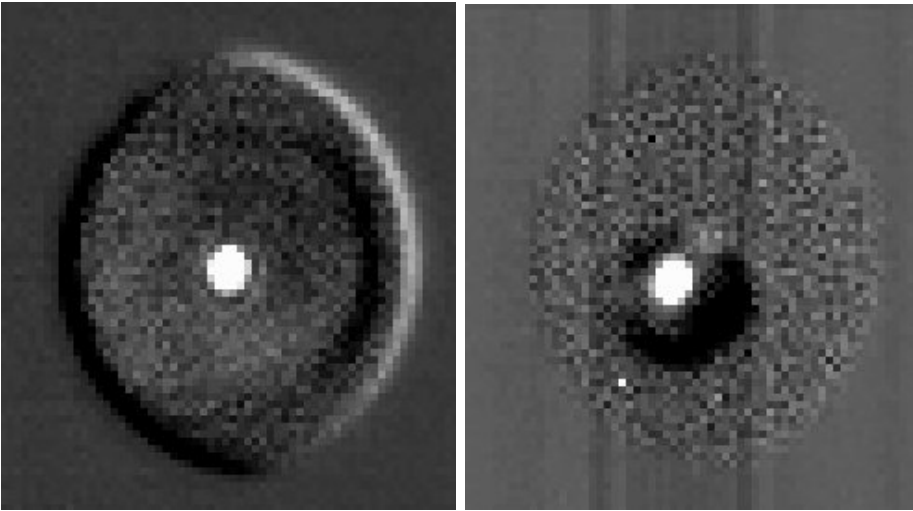


Figure 2: MIDI acquisition with UT (left) and VCM-equipped AT (right). The images represent the difference between the mean raw target and sky frames. Within the cold-stop, the FOV with an UT is 2 arcseconds in diameter, and tunnel emission is confined to the very edge of the FOV. The PSF covers the same number of pixels for UTs and ATs. There is also significant FOV with the AT.

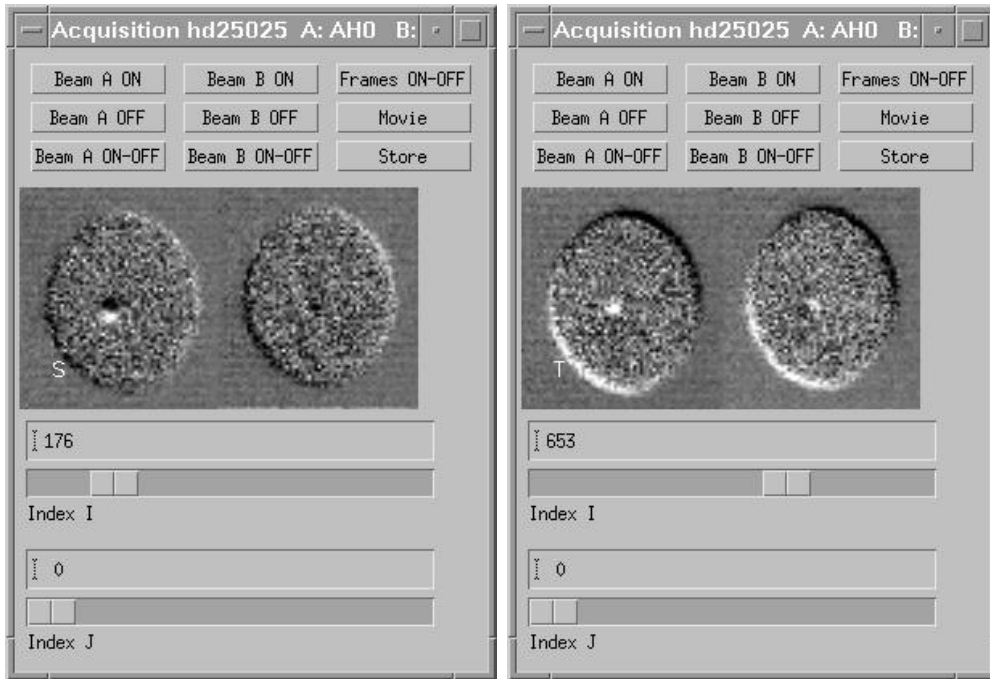


Figure 3: Two MIDI acquisition frames, each showing AT1 on the left and AT3 on the right. On the left, pointing is to the sky, on the right to the target. In both cases, a mean sky frame has been subtracted. The FOV of AT1 here is small but non-zero, and so the edge which indicates the transition into tunnel emission encroaches on the target. Small registration errors can cause large residual background variations in the chopped frames. This is the reason for the occurrence of the artefacts (here even in a sky frame as shown on the left), even if sometimes the image looks clean (as in the second frame). If the FOV is close to zero, and tunnel emission fills in the FOV, there is only a very small region showing the target signal which consequently has a narrow profile.

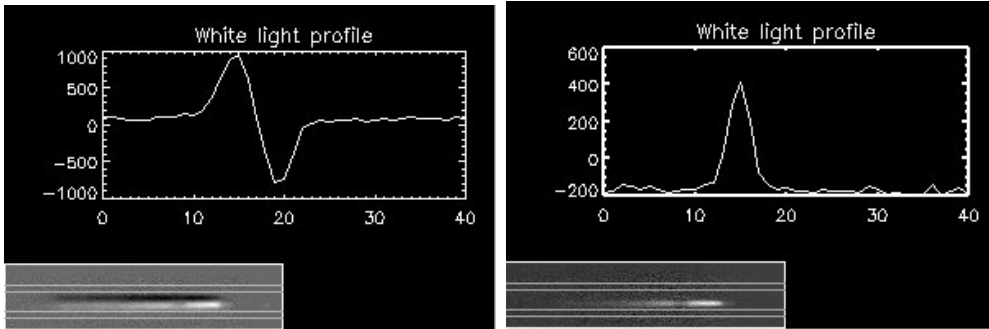


Figure 4: Chopped photometry frames and cuts through the white light average. Left: “P-Cygni” profile (AT1); right: “Normal” profile (AT3). Note that the narrow profile for AT3 does not correspond to the PSF, rather to the FOV. The spectra have 171 columns along the dispersion direction, and 41 rows in the spatial direction.

4 Photometry

Photometry is needed to normalize the raw correlated flux measured in the fringe exposures. The same dispersive element is used as in the fringe exposure. As with the acquisition, chopping is on, and the spectra are extracted using a mask which is fit to the maxima of the spatial profiles along the dispersion direction. Just like the acquisition frames, the chopped spectra show, mostly for AT1 with the slightly larger FOV, a distorted profile (“P-Cygni” profile, see Fig 4). With such a distortion, it is immediately obvious that a reliable flux cannot be extracted. Strong systematic trends in the visibilities have always been traced back to distortions in the flux spectra.

5 Field of view jitter

The bright and dark crescents which can be seen at the edge of the cold stop (Fig. 2) were early-on interpreted as due to an oscillation of the MIDI detector relative to the incoming beam. This oscillation is caused by the cooler of MIDI which is always on, and has a period of 1 s. Cyclic variations on a longer time scale with larger amplitudes are present as well, but their source has not yet been identified. Rather than trying to analyse individual chopped frames, the raw sky and target frames can be used to measure the

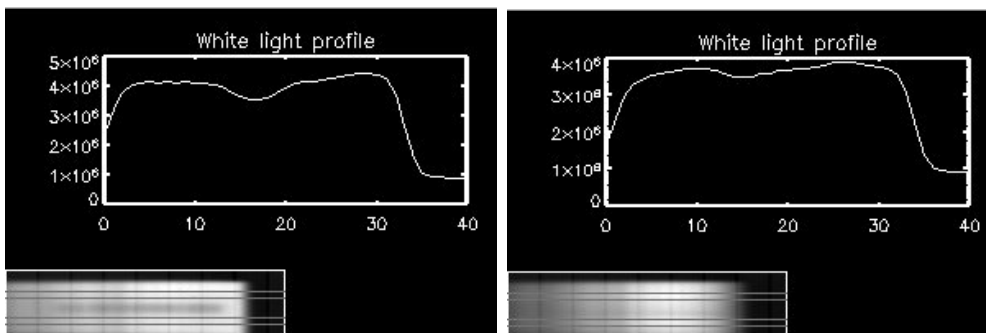


Figure 5: Raw spectra and white light profile for AT1 (left) and AT3 (right). (The thin lines outline “sky” windows used by the EWS package for residual sky subtraction; these are obviously badly placed in this case.)

oscillation, at least the component along the slit. Examples of these are shown in Fig. 5. For the measurement of the jitter, both target and sky frames are suitable.

Therefore, an attempt was made to measure the jitter of MIDI, first by fitting the emission dip due to sky near the center of each frame. The results are shown in Fig. 6.

Another way to determine the relative offsets between successive raw frames is to cross-correlate their profiles with a mean profile. The results are similar to the FOV fit results, and are shown in Fig. 7.

6 Corrective action in data reduction

The basic idea would be to recenter the frames before subtracting sky from target frames. Then, the registration errors at the FOV edges would not produce the distortions. However, due to the background being several orders of magnitude stronger than the target signal and the pixel to pixel gain variations of the MIDI detector which are not known, it is better to chop frames separately in different offset bins and then average the chopped frames. Using this method, however, only the jitter along the slit can be measured and corrected for, the jitter perpendicular to the slit remains a source of background contamination.

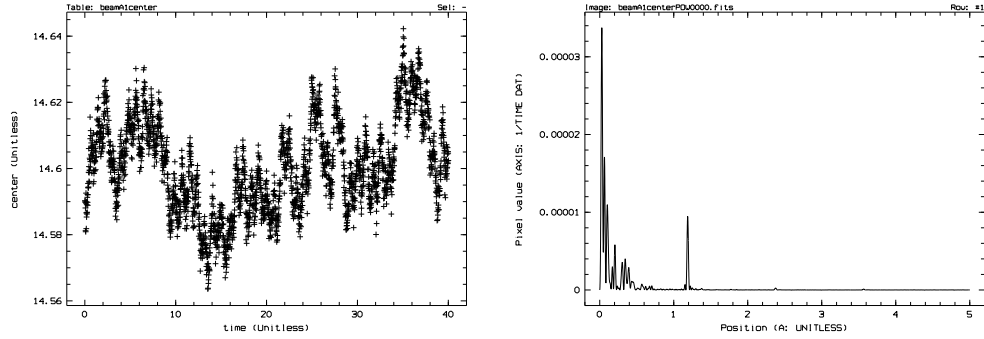


Figure 6: Left: The position of the center of the FOV as a function of frame number. Right: cleaned powerspectrum of the FOV center. The 1 s periodicity is clearly present. Note that the unit is not exactly 1 Hz since the frames were assigned multiples of the DIT as time-stamp, neglecting read-out time.

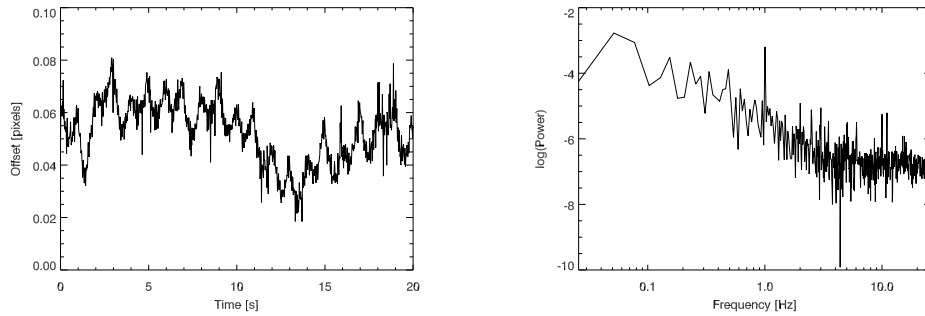


Figure 7: Left: The offsets of successive frames derived by cross-correlation. Right: (Unprocessed) power spectrum of frame offsets. For comparison with Fig. 6 note that only the first 20 seconds of data are shown.

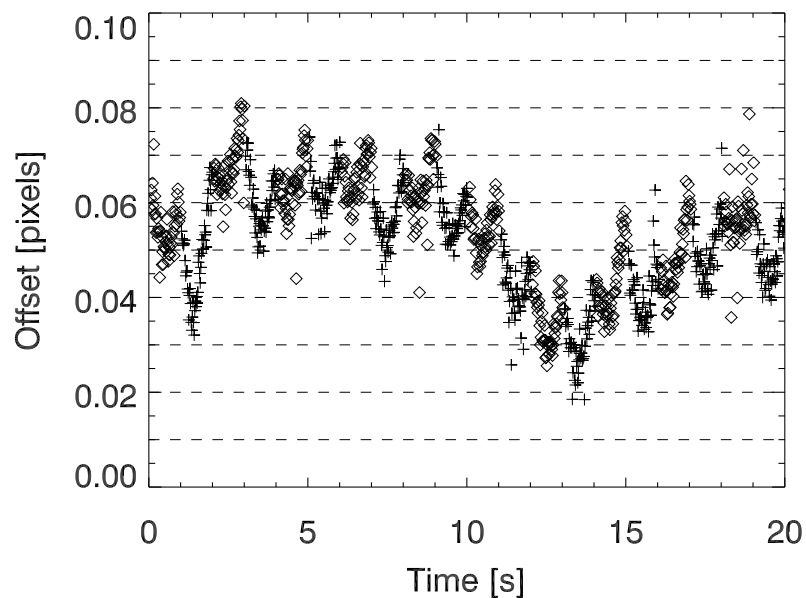


Figure 8: A short portion of AT1 frame offsets and the placement of bins (dashed lines). Sky frame offsets are denoted with plus symbols, target frames with diamonds.

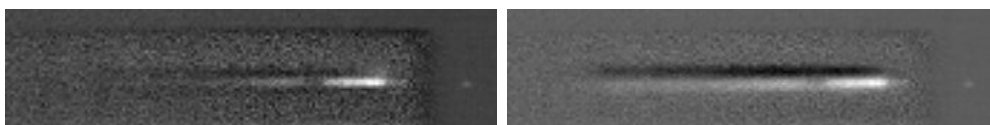


Figure 9: Left: average chopped frame after chopping frames separately in offset bins of width 0.01 pixels. Right: control average without recentering. The stellar signal is clearly seen now (left image), but still is seated in a dip due to background variations, presumably the jitter perpendicular to the slit not corrected for.

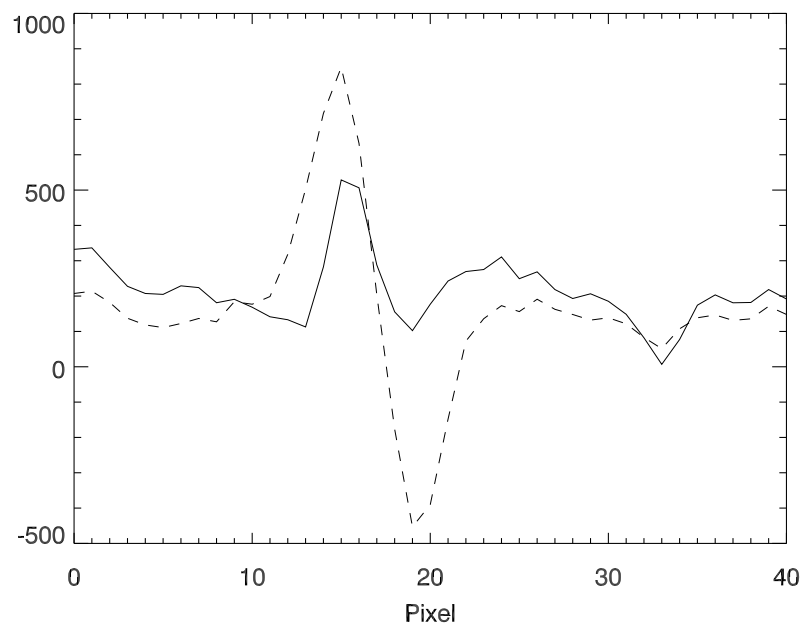


Figure 10: White light profiles of original chopped frame (dashed line) and recentered chopped frame. This is the same target (HD 25025, Jan 1, 2006) as shown in Fig. 4

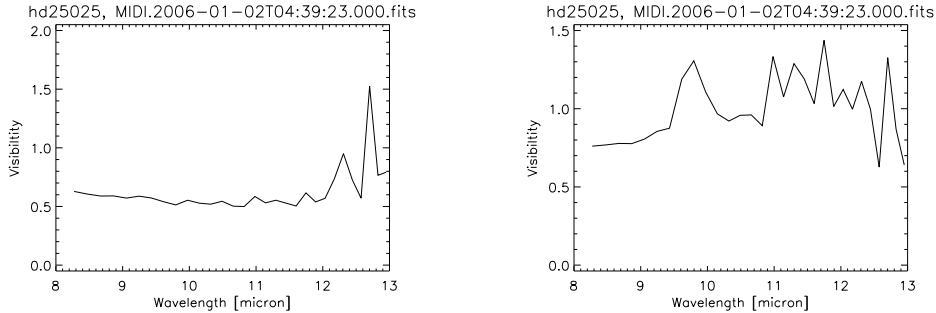


Figure 11: Visibility without (left) and with (right) binned averaging, for the observation of HD 25025 on Jan 1, 2006.

7 Effects on the visibility from the application of the algorithm

The improvements for the visibilities are inconsistent. The systematic effect of the distorted photometric profile is to lower the visibility. The algorithm, as shown above, tends to restore the source profile, and the visibility is raised as a consequence. However, due to the low flux caused by the small field of view, systematic errors tend to get magnified, as shown in Fig. 11.

Looking at data from several nights during P76, the number of photometric observations with severe loss of flux is significant, in which cases the photometry cannot be restored at all.

The binned averaging algorithm should not change a profile which does not have a contribution due to strong systematic background fluctuations such as the FOV edges. Therefore, observations in which both beams suffer from “zero” FOV can, if reduced traditionally, show the limits of the data quality (see Fig. 12).

8 Application of the algorithm on all calibrator data

We processed all MIDI/AT calibrator data recorded in PRISM/HIGH_SENS mode without the VCMs from 12 October 2005 to 18 January 2006 during

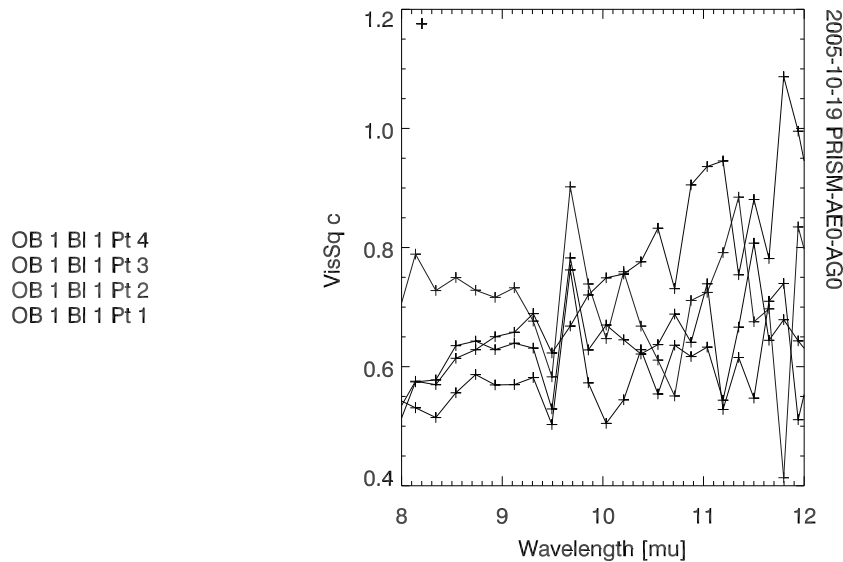


Figure 12: Visibilities of the calibrator HD 25025 observed Oct 18, 2005, on E0-G0 with “zero” FOV in both beams.

service mode operations. Results are posted at <http://www.sc.eso.org/~chummel/midi/lab/lab.html>. Most calibrator stars can be considered point sources. As the MIA+EWS software and the modifications have not been finalized for their use with AT/MIDI data, these reductions must be considered as preliminary.

The results based on the modified algorithms seem to be somewhat more consistent than those based on the regular MIA algorithms. However, also the resulting visibility amplitudes based on the modified algorithms are often inconsistent with the expected shape and amplitude for a calibrator (for instance giving visibility values larger than unity or very low visibility amplitudes) in an obvious way. Based on the analysis with the modified algorithms, we de-selected all these calibration star data that are obviously faulty and kept only those calibration star OBs that give a visibility function approximately consistent with the expected shape and amplitude for a calibrator.

Out of 104 calibration star data, a total of 22 calibration star visibility data were kept (21%), 14 out of 39 for the E0-G0 baseline (36%), 8 out of 52 for the G0-H0 baseline (15%), none out of the 13 for the G0 K0 baseline. Note, however, that only obviously faulty visibility amplitudes were excluded,

and that the remaining ones often still show a very noisy shape and may not be scientifically useable. Remaining visibility data were obtained for the calibration stars HD 25025, HD 48915 (Sirius), Procyon, and HD 82668 with fluxes of 110 Jy, 143 Jy, 79 Jy, and 73 Jy, respectively.

Tables 1 and 2 list these remaining calibration star data. Figure 16 shows the results (modified algorithm) for these remaining calibration star OBs per baseline. It can be seen that these remaining visibility data are consistent with their own mean and with the expected shape and amplitude for a calibrator.

9 Conclusions

The data taken without the VCM have been analyzed using the modified data reduction algorithms. A fraction of 22% of all calibration star data show a visibility function that is not obviously faulty, but often still very noisy. Despite these limitations some of these data would still have scientific value.

10 Preliminary results with the use of the VCMs

The FOV improvement afforded by the VCMs is significant and makes operations with the ATs quite similar to the UTs. However, regular pupil alignment using M10 and a new and quick procedure with ARAL are used to keep the FOV edges away from the target. (Should the target ever end up too close to the FOV edge, the above described algorithm could be used to remove some of the systematic errors caused.) In the following Figs. 13 and 14 we compare the increase in throughput, which is on the order of 10 to 20 times.

The resulting improvement of the visibility can be seen in Fig. 15.

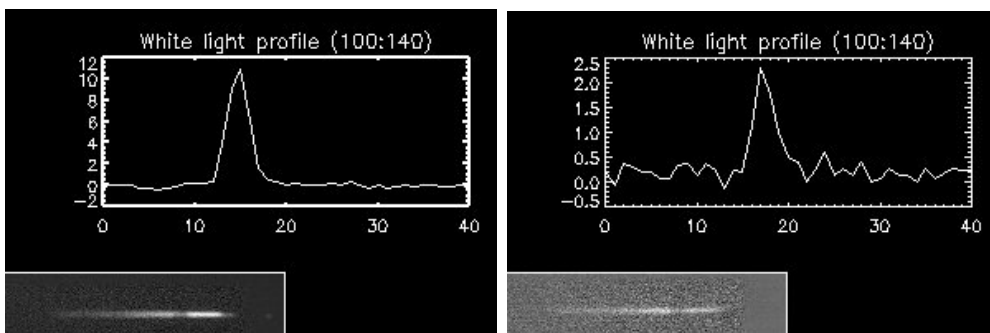


Figure 13: Photometry of a target taken without VCMs, for shutters A and B.

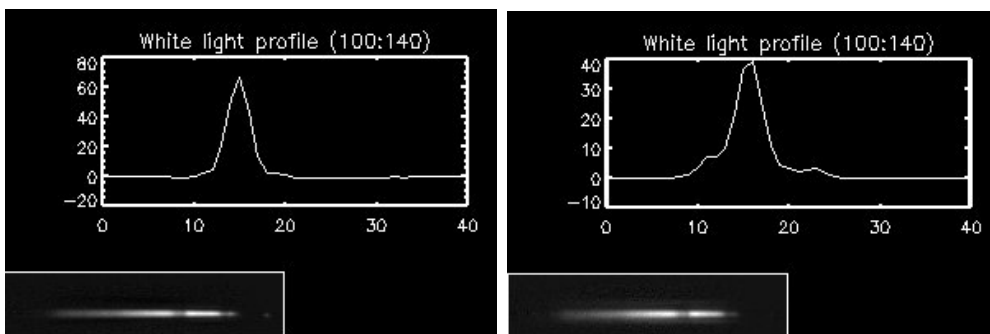


Figure 14: Photometry of the same target taken with VCMs, for shutters A and B.

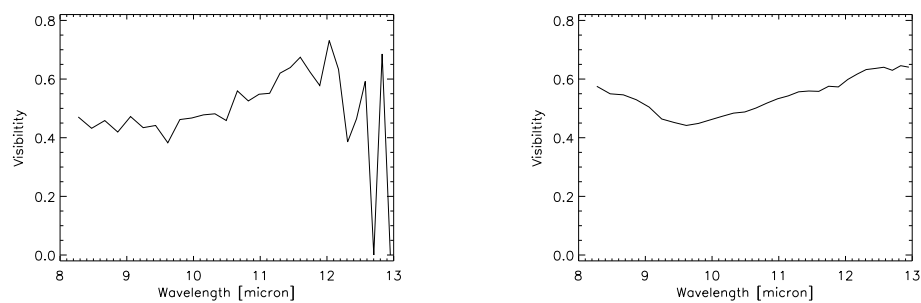


Figure 15: Visibilities of the same target without VCMs (left) and with VCMs (right).

Table 1: Calibration star data on the E0-G0-16m baseline that lead to a visibility function approximately consistent with the expected one for a calibrator.

NIGHT=2005-10-16	OB=200153281	hd25025
NIGHT=2005-10-17	OB=216192	HD48915
NIGHT=2005-10-17	OB=210591	procyon
NIGHT=2005-10-18	OB=213589	hd25025
NIGHT=2005-10-18	OB=200153294	hd25025
NIGHT=2005-10-18	OB=200153297	hd25025
NIGHT=2005-10-18	OB=213589	hd25025
NIGHT=2005-10-19	OB=200153313	hd25025
NIGHT=2006-01-10	OB=200154975	CAL-04:35+16
NIGHT=2006-01-11	OB=210608	hd25025
NIGHT=2006-01-11	OB=210620	hd25025
NIGHT=2006-01-14	OB=210604	hd25025
NIGHT=2006-01-14	OB=213560	hd82668
NIGHT=2006-01-15	OB=210623	hd25025
NIGHT=2006-01-15	OB=213621	hd25025

Table 2: Calibration star data on the G0-H0-32m- baseline that lead to a visibility function approximately consistent with the expected one for a calibrator.

NIGHT=2005-11-18	OB=-1557947307	no corresponding science OB
NIGHT=2005-11-18	OB=216194	not reduced
NIGHT=2005-11-19	OB=200153649	no corresponding science OB
NIGHT=2005-11-20	OB=214447	hd48915
NIGHT=2006-01-01	OB=213742	hd25025
NIGHT=2006-01-04	OB=213675	hd82668
NIGHT=2006-01-05	OB=210567	hd25025
NIGHT=2006-01-05	OB=213741	hd25025

Figure 16: Visibility amplitudes (modified algorithm) for the remaining calibration star OBs per baseline (top E0-G0, middle G0-E0, bottom G0-H0) Not all calibrators are from CalVin.

